A DC Hybrid Active Power Filter and Its Nonlinear Unified Controller Using Feedback Linearization

Li, Gaoxiang; Luo, An; He, Zhixing; Ma, Fu jun; Chen, Yandong; Wu, Wenhua; Zhu, Zhen; Guerrero, Josep M.

Published in:
IEEE Transactions on Industrial Electronics

DOI (link to publication from Publisher):
10.1109/TIE.2020.2996147

Publication date:
2021

Document Version
Accepted author manuscript, peer reviewed version

A DC Hybrid Active Power Filter and Its Nonlinear Unified Controller Using Feedback Linearization

Gaoxiang Li, An Luo, *Senior Member, IEEE*, Zhixing He, *Member, IEEE*, Fujun Ma, *Member, IEEE*, Yandong Chen, *Senior Member, IEEE*, Wenhua Wu, Zhen Zhu, and Josep M. Guerrero, *Fellow, IEEE*

***Abstract*—In current power system, the conversion between DC and AC is widely existing and dc side harmonic problem is prominent. To suppress the second-harmonic current (SHC) at the dc side of single-stage single-phase inverter, a dc hybrid active power filter (DC-HAPF) structure is presented, which composes of bidirectional dc-dc circuit based active power filter and CL passive filter. Here, the CL passive filter is used to mitigate the high frequency harmonics and the active power filter is applied to compensate the low frequency harmonic current. Meanwhile, the influence of filter parameters on harmonic suppression is analyzed based on the average switching model. In addition, for the control of the DC-HAPF, a nonlinear unified controller via feedback linearization is proposed, where the voltage and current dual-loop control is converted to a single-loop control of energy. By analyzing the control system stability and DC-HAPF's performance, appropriate control parameters are selected. To verify the feasibility of the proposed topology and control strategy, a 500W single-stage single-phase inverter with the DC-HAPF is built and a good performance of dc side harmonic suppression has been achieved.**

***Index Terms*—Second harmonic current, hybrid active power filter, feedback linearization, single-stage single-phase inverter.**

I. Introduction

HARMONIC elimination is great significance for improving power quality, reducing power loss and enhancing grid reliability. Power electronic based inverters are widely used in current power systems. According to the topology, the inverters can be classified into the single-phase inverters and the three-phase inverters. Compared with the three-phase inverters, the signal-phase inverters are mainly used in systems that with low power range (<10kW) [1]. As for the low-voltage small-power micro-grids, such as home micro-grids generally adopt single-phase power supply structure, and it is easily vulnerable to external devices. So the improvement of power quality for single-phase power supply is important. According to the instantaneous power theory, there is power ripple at twice the fundamental frequency ($2f_o$) for the output power of the single-phase inverter, which results in the second-harmonic current (SHC) at the dc-side of the single-phase inverter [2]. The SHC will cause additional power loss and higher current stress. Moreover, for the dc voltage sources, such as batteries, photovoltaic cells and fuel cells, the SHC will shorten their lifetime and reduce energy conversion efficiency. A large capacitor is usually used to suppress the dc-side harmonics of single-phase inverter, but it has the disadvantages of large size and poor performance. Therefore, it is necessary to further study the dc-side harmonic suppression for the single-phase inverters.

Moreover, according to the structure, the single-phase inverters can be categorized into the single-stage inverters and the two-stage inverters. [1] and [2] offered an overview of the low frequency power decoupling of single-phase inverters and the dc-side harmonic suppression methods. For the two-stage single-phase inverters, the SHC is mainly mitigated by improving control methods [3]-[14]. In [3], a SHC reduction method is proposed for the dc–dc converters, which regulates the dc-bus voltage. A virtual series impedance, which has high impedance at $2f_o$ while low impedance at other frequencies, is presented for increasing the impedance of the boost-diode branch or the boost-inductor branch at $2f_o$ [4]. Various control schemes have been presented for mitigating the SHC in the buck-derived front-end dc–dc converter [5]-[10] and the SHC is suppressed in the control link of dc-dc converter. In [11]-[14], different control strategies are presented for mitigating the low frequency current ripples, where a boost-type differential inverter made up of two bidirectional boost converters is adopted. For the single-stage single-phase inverters, the SHC can be suppressed by adding filter [15]-[21]. In [15], a ripple power port is designed to manage energy storage and decouple capacitor ripple from power ripple. In [16], a bidirectional buck-boost converter is used as the ripple energy storage circuit, which can effectively reduce the energy storage capacitance. A current pulsation smoothing parallel active filter (CPS-PAF) is used for the advantage that it requires a small film capacitor [17]. In [18], an integrator is added into the control loop to inject the ripple current into the dc-link and restrain the dc component of the current reference. In [19], a rectifier is designed for the mitigation of power ripple at twice the line frequency and the dc power is in series with an inductor. A new power decoupling circuit applied to the single-phase current source converter (SCSC) is proposed [20]. An active buffer without a large inductor and capacitor in the dc-link part is designed [21]. An in all, to deal with the SHC, different ways are proposed based on the different structures.

Manuscript received August 5, 2018; revised August 8, 2019 and March 20, 2020; accepted May 7, 2020. This work was supported by the National Key Research and Development Program of China under Grant 2017YFB0902000; State Grid Project SGXJ000KXJS1700841 and Hunan Provincial Natural Science Foundation of China 2019JJ50006. (*Corresponding author: Fujun Ma*.)

G. Li, A. Luo, Z. He, F. Ma, Y. Chen, W. Wu and Z. Zhu are with the College of Electrical and Information Engineering, Hunan University, Changsha 410082, China (e-mail: ligaoxiang5@163.com; an_luo@126.com; hezhixing-mail@163.com; mafujun2004@163.com; yandong_chen@hnu.edu.cn; wenhua_5@163.com; 332120507@qq.com).

J. M. Guerrero is with the Department of Energy Technology, Aalborg University, Aalborg 9220, Denmark (e-mail: joz@et.aau.dk).

This article has been accepted for publication in a future issue of this journal, but has not been fully edited. Content may change prior to final publication. Citation information: DOI 10.1109/TIE.2020.2996147, IEEE Transactions on Industrial Electronics

However, the cooperative working mechanism and control performance between the dc active power filter and the passive filter for suppressing the dc-side harmonics are rarely studied.

Feedback linearization is an advanced nonlinear control method without neglecting the higher order terms in the linearization process. This technique has been successfully applied to the areas of power electronic converters [22-24]. By applying exact feedback linearization theory, a nonlinear control strategy is presented for single-phase active power filter [25]. A new feedback linearization approach is proposed, which yields a decoupled linear induction motor (IM) model with two state variables: torque and stator flux magnitude [26]. In [27], a simplified feedback linearization of single-phase active power filter using sliding mode control is proposed. An innovative simplified feedback linearization (SFL) control strategy is designed for the PV inverter with the LCL filter [28]. For achieving excellent performance under various operating conditions, a controller based on the partial feedback linearization is proposed [29]. A controller is designed based on the partial feedback linearization to regulate the line voltage by providing reactive power compensation [30]. In [31], a nonlinear damping controller is designed based on partial feedback linearization for mitigating sub-synchronous oscillation. Compared with traditional controller, the controllers based on feedback linearization have a good dynamic and steady performance. However, owing to the different circuit structures and control targets, the feedback linearization-based controllers also are different. Therefore, it is usually necessary to design the appropriate controller based on the specific application scenarios.

In this paper, for distinguishing the traditional ac hybrid active power filter (HAPF), the concept of dc hybrid active power filter (DC-HAPF) is presented. In addition, to suppress the SHC and high frequency harmonics at the dc side of single-stage single-phase inverters, a DC-HAPF topology composed of bidirectional dc-dc circuit based active power filter and CL filter, is proposed. For the control of DC-HAPF, a nonlinear unified controller using feedback linearization is proposed. The rest of this paper is organized as follows. The single-stage single-phase inverter with the proposed DC-HAPF is introduced in Section II. In addition, the characteristics of the DC-HAPF are analyzed based on the average switching model. After that, Section III introduces the nonlinear unified controller via feedback linearization and the design method of control parameters. Experimental results are presented in Section IV.

II. DC Hybrid Active Power Filter and Its Filtering Characteristics

Fig.1 shows the configuration of single-stage single-phase inverter with the designed DC-HAPF. The CL filter composes of C_1 and L_1, where C_1 is also the dc-bus capacitor for the single-stage inverter. The dc active power filter is based on the bidirectional dc-dc converter, which composes with L_2, C_2, S_5 and S_6. The current i_{inv} contains a lot of harmonic components, especially the SHC and high frequency harmonics associated with the switching frequency. The CL filter can suppress the high frequency harmonic currents effectively, but it has a poor effect on the SHC. After CL filtering, the harmonic current in i_{L1} is mainly low-frequency harmonic current, which can be compensated by the APF.

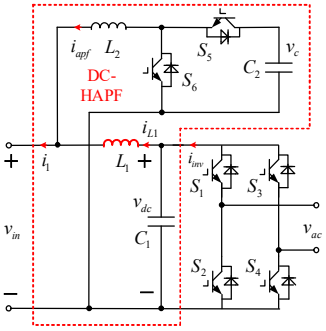

Fig.1. Configuration of single-stage single-phase inverter with DC-HAPF.

According to Fig.1, by using state-space average method, the mathematical model of APF can be expressed as,

$$\begin{cases} L_2 \dfrac{di_{apf}}{dt} = v_{in} D_k + (v_{in} - v_c) D_k^{'} \\ C_2 \dfrac{dv_c}{dt} = i_{apf} D_k^{'} \end{cases} \tag{1}$$

where i_{apf} is the output current of APF; v_{in} is the input voltage for APF; v_c is the voltage of C_2; D_k is the duty-cycle of S_6 in the switching period k, and $D'_k+D_k=1$, expressed as,

$$D_k = 1 - \frac{v_{in}}{v_c} \tag{2}$$

Applying the Laplace Transformation, (1) can be rewritten as,

$$\begin{cases} i_{apf} = \left[v_{in} D_k + (v_{in} - v_c) D_k^{'} \right] / (sL_2) \\ v_c = i_{apf} D_k^{'} / (sC_2) \end{cases} \tag{3}$$

According to two-port network theory, the bidirectional dc-dc circuit based APF at the dc side of single-phase inverter can be equivalent to an impedance. According to (3), the equivalent impedance of the APF can be obtained as,

$$Z_{apf}(s) = \frac{v_{in}}{i_{apf}} = \frac{L_2 C_2 s^2 + D_k^{'2}}{sC_2} \tag{4}$$

By setting L_2=1mH, C_2=2mF and D_k=0.1, the Bode diagram for Z_{apf}(s) is depicted, as shown in Fig.2.

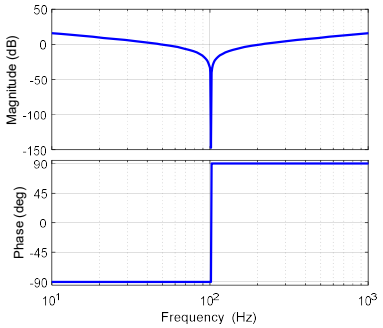

Fig.2. Bode diagram of Z_{apf}(s).

Seen from Fig.2, the magnitude of Z_{apf}(s) is very low at $2f_o$, which likes a notch filter. This implies that the equivalent impedance of the APF is very small at $2f_o$. At other frequencies, the magnitude of Z_{apf}(s) is much bigger than that of Z_{apf}(s) at $2f_o$. It means that the APF can provide a channel for SHC and hinder the passing of dc current.

According to (4), the characteristics of Z_{apf}(s) are determined by three parameters L_2, C_2 and D_k. Because C_2 not only is a filter

This article has been accepted for publication in a future issue of this journal, but has not been fully edited. Content may change prior to final publication. Citation information: DOI 10.1109/TIE.2020.2996147, IEEE Transactions on Industrial Electronics

capacitor, but also the dc-bus capacitor for the single-stage inverter. So, C_2 is designed based on the dc voltage fluctuation requirement. In order to better design the parameters L_2 and D_k, the amplitude-frequency characteristics of Z_{apf}(s) under different L_2 and D_k are showed in Fig.3.

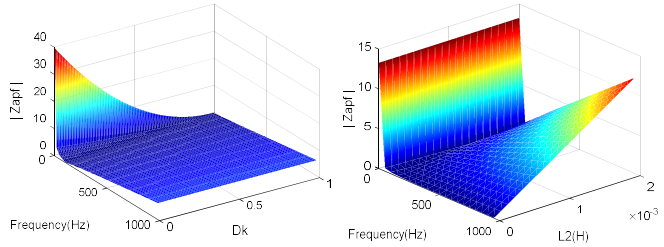

Fig.3. Amplitude-frequency characteristics of Z_{apf}(s) under different parameters. (a) Under different D_k. (b) Under different L_2.

According to Fig.3(a), the amplitude of Z_{apf}(s) increases significantly with the decrease of D_k in the low-frequency part (lower than $2f_o$). Similarly, according to Fig.3(b), the amplitude of Z_{apf}(s) raises rapidly with the increase of L_2 in the high-frequency part (higher than $2f_o$). No matter the increase of D_k or L_2, the amplitude ratio of Z_{apf}(s) is always low at the frequency $2f_o$. Hence, the impedance characteristics of Z_{apf}(s) can be improved by designing the value of D_k and L_2.

Replacing the APF with the equivalent impedance Z_{apf}(s), the simplified circuit topology of Fig.1 can be depicted in Fig.4, where V_{in} is the dc voltage source and R_0 is its internal resistance.

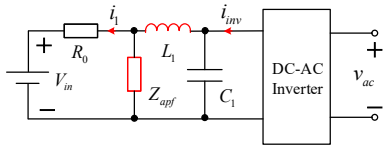

Fig.4. The simplified circuit topology of single-stage single-phase inverter with DC-HAPF.

It is well known that the downstream single-phase inverter can be equivalent to a dc current source I_{dc} in parallel with an SHC source I_{SHC} if neglecting the switching harmonics. The circuit topology of the single-stage single-phase inverter with different filters can be further simplified, as shown in Fig.5.

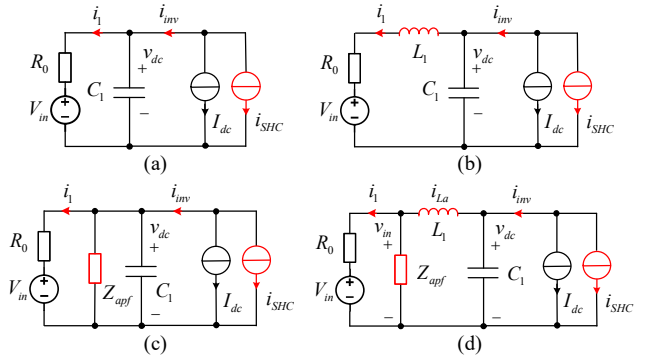

Fig.5. The simplified circuit of the single-stage single-phase inverter with different filters. (a) With filter C. (b) With filter CL. (c) With filter C+APF. (d) With filter CL+APF.

According to Fig.5, the equivalent control diagrams of single-stage single-phase inverter with different filter can be depicted in Fig.6.

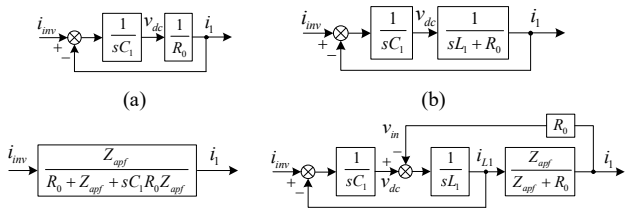

Fig.6. Equivalent control diagrams of single-stage single-phase inverter with different filters. (a) With filter C. (b) With filter CL. (c) With filter C+APF, (d) With filter CL+APF.

According to Fig.6(a), the transfer function from i_{inv} to i_1 can be expressed as,

$$i_1 = \frac{1}{sC_1R_0 + 1} i_{inv} \tag{5}$$

Similarly, from Fig.6(b), the transfer function from i_{inv} to i_1 can be expressed as,

$$i_1 = \frac{1}{sC_1\left(sL_1 + R_0\right) + 1} i_{inv} \tag{6}$$

Similarly, from Fig.6(c), the transfer function from i_{inv} to i_1 can be expressed as,

$$i_1 = \frac{Z_{apf}}{R_0 + Z_{apf} + sC_1R_0Z_{apf}} i_{inv} \tag{7}$$

Similarly, from Fig.6(d), the transfer function from i_{inv} to i_1 can be expressed as,

$$i_1 = \frac{Z_{apf}}{\left(s^2L_1C_1 + 1\right)\left(Z_{apf} + R_0\right) + sC_1R_0Z_{apf}} i_{inv} \tag{8}$$

By setting L_1 =0.1mH, C_1=1.5mF, L_2 =1mH, C_2 =2mF, R_0=0.01ohm, and D_k=0.1, the Bode plots for (5), (6), (7) and (8) are depicted in Fig.7.

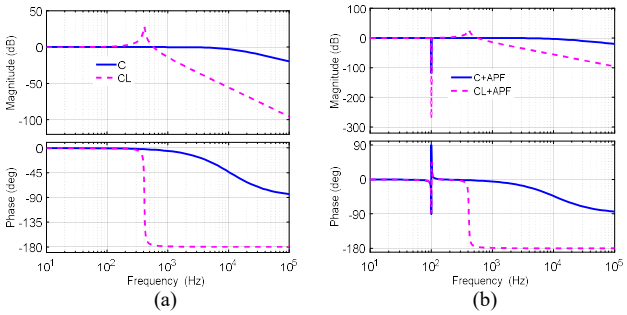

Fig.7. Bode diagrams of the transfer functions from i_{inv} to i_1. (a) Bode diagrams of (5) and (6). (b) Bode diagrams of (7) and (8).

As seen from Fig.7(a), the magnitude of (5) is higher than that of (6) in the high frequency part. It shows that CL filter has a good effect on suppressing the high-frequency harmonic current. Seen from Fig.7(b), the magnitude of (7) and (8) are very low at the frequency $2f_o$ and it shows that the APF can suppress SHC effectively. In addition, the magnitude of (7) is higher than that of (8) in the high-frequency part, and it shows that CL+APF has a better control effect than C+APF for high frequency harmonics. Therefore, the proposed DC-HAPF integrates the merits of both active power filter and passive filter.

Seen form (8), the internal resistance R_0 can affect the filtering effect. Similarly, the values of D_k and L_1 also have a great influence on the performance of DC-HAPF. To better analyze

This article has been accepted for publication in a future issue of this journal, but has not been fully edited. Content may change prior to final publication. Citation information: DOI 10.1109/TIE.2020.2996147, IEEE Transactions on Industrial Electronics

the influence of the D_k, L_1 and R_0 on the filtering effect, the amplitude-frequency characteristics of (8) under different D_k, L_1 and R_0 can be depicted in Fig.8.

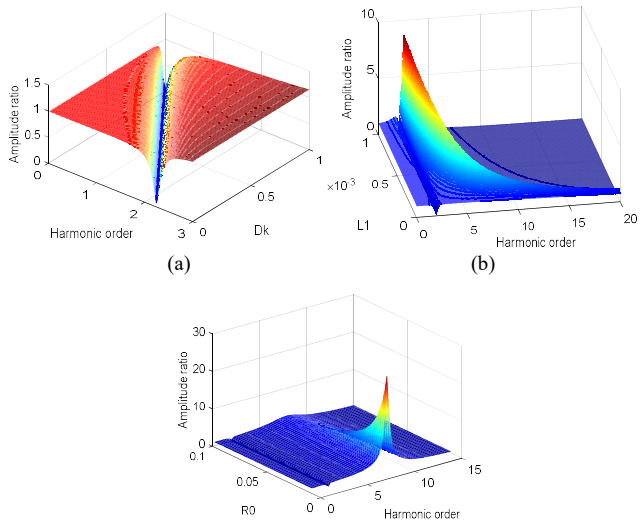

Fig.8. Amplitude-frequency characteristics of (8) under different parameters. (a) Under different D_k, (b) Under different L_1, (c) Under different R_0.

Seen from Fig.8(a), the trap frequency of (8) gradually increases with the decrease of D_k in the low frequency part. Similarly, according to Fig.8(b), the amplitude of (8) significantly decreases with the increase of L_1 in the high-frequency part but rapidly increases in the low frequency part. No matter the L_1 increases or not, the amplitude of (8) stays the same at the frequency $2f_o$. Hence, the SHC can be improved by designing the values of D_k and L_1. In addition, as shown in Fig.8(c), the amplitude of (8) decreases with the increase of impedance R_0. It shows that the increase of the resistance R_0 can suppress the harmonic current. However, the resistance R_0 is determined by the characteristics of the dc voltage source V_{in}, and artificially increasing the resistance R_0 will increase the additional power loss.

III. Nonlinear Unified Control via Feedback Linearization

In order to improve the control performance of system, the nonlinear unified controller using feedback linearization is designed in Fig.9. Applying feedback linearization theory, the appropriate new state variables are obtained and the inverse function is established. According to the new state variables, the nonlinear system can be converted into the linear system. Then, a linear system controller is designed based on the obtained linear system. Finally, according to the inverse function, the primary control variable can be obtained by the state variables and control variable of the linear system, which can realize the control of the nonlinear system.

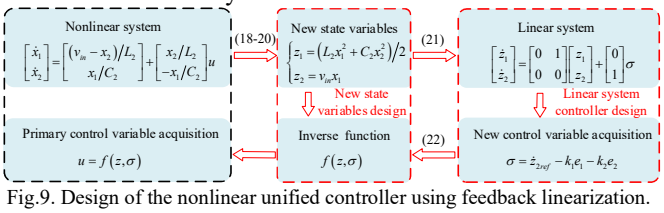

Fig.9. Design of the nonlinear unified controller using feedback linearization.

Replacing the duty-cycle D_k by the input variable u, (1) can be rewritten as,

$$\begin{cases} \dfrac{di_{apf}}{dt} = \dfrac{v_{in}-v_c}{L_2} + \dfrac{v_c}{L_2}u \\ \dfrac{dv_c}{dt} = \dfrac{i_{apf}}{C_2} - \dfrac{i_{apf}}{C_2}u \end{cases} \tag{9}$$

According to (9), selecting $\boldsymbol{x}=[x_1, x_2]=[i_{apf}, v_c]$ as state variables, $y_x=h(\boldsymbol{x})=x_1$ as output and $u=D_k$ as the input, the single-input single-output (SISO) nonlinear system based on differential geometry method can be obtained as,

$$\begin{cases} \dot{x} = f(x) + g(x)u \\ y_x = h(x) = x_1 \end{cases} \tag{10}$$

where

$$f(x) = \begin{bmatrix} \dfrac{v_{in}-x_2}{L_2} \\ \dfrac{1}{C_2}x_1 \end{bmatrix} \tag{11}$$

$$g(x) = \begin{bmatrix} \dfrac{1}{L_2}x_2 \\ \dfrac{-1}{C_2}x_1 \end{bmatrix} \tag{12}$$

where, $f(x)$ and $g(x)$ are controllable matrices. According to (11), (12) and Lie derivatives [28], there is,

$$ad_f g(x) = \frac{\partial g(x)}{\partial x} f(x) - \frac{\partial f(x)}{\partial x} g(x) = \begin{bmatrix} 0 \\ \dfrac{-v_{in}}{L_2 C_2} \end{bmatrix} \tag{13}$$

Combining (12) and (13), there is,

$$\begin{bmatrix} g(x) & ad_f g(x) \end{bmatrix} = \begin{bmatrix} \dfrac{x_2}{L_2} & 0 \\ \dfrac{-x_1}{C_2} & \dfrac{-v_{in}}{L_2 C_2} \end{bmatrix} \tag{14}$$

Seen from (14), the rank of matrix (14) is 2, and the order of system (10) is also 2. Based on feedback linearization theory and differential geometry method, the system (10) can be precisely linearized. Thus, it can be determined that there is an output function making the relative order of the system be equal to the dimension of the system. The characteristic of system (10) is that it is nonlinear for the state variable x, but linear for the control variable u.

Applying Lie derivatives [28], according to (10)-(12), there is,

$$\begin{cases} L_f h(x) = \dfrac{\partial h(x)}{\partial x} \cdot f(x) = \dfrac{v_{in}-x_2}{L_2} \\ L_g h(x) = \dfrac{\partial h(x)}{\partial x} \cdot g(x) = \dfrac{1}{L_2}x_2 \end{cases} \tag{15}$$

According to (15), the relative order of the system (10) is 1, not equal to the dimension of the system. The original system (10) cannot be precisely linearized owning to the output function. It is necessary to reconstruct a new output function to re-

This article has been accepted for publication in a future issue of this journal, but has not been fully edited. Content may change prior to final publication. Citation information: DOI 10.1109/TIE.2020.2996147, IEEE Transactions on Industrial Electronics

alize the precise feedback linearization. Supposing the new output function is ω(x), it needs to satisfy the following differential equation,

$$\frac{\partial\omega(x)}{\partial x}g(x)=0 \tag{16}$$

According to (12) and (16), there is,

$$\frac{\partial\omega(x)}{\partial x}g(x)=\frac{\partial\omega(x)}{\partial x_1}\frac{1}{L_2}x_2-\frac{\partial\omega(x)}{\partial x_2}\frac{1}{C_2}x_1=0 \tag{17}$$

For (17), a solution can be obtained,

$$\omega(x)=\frac{L_2x_1^2+C_2x_2^2}{2} \tag{18}$$

Clearly, the new output function is APF's energy function, which has a clear physical meaning.

According to (11) and (18), there is,

$$L_f\omega(x)=v_{in}x_1 \tag{19}$$

Combing (18) and (19), the coordinate transformation can be derived as,

$$\begin{cases} z_1=\omega(x)=\dfrac{L_2x_1^2+C_2x_2^2}{2} \\ z_2=L_f\omega(x)=v_{in}x_1 \end{cases} \tag{20}$$

By coordinate transformation, (10) can be described as,

$$\begin{cases} \dot{z}=\begin{bmatrix}0&1\\0&0\end{bmatrix}z+\begin{bmatrix}0\\1\end{bmatrix}\sigma \\ y_z=z_1 \end{cases} \tag{21}$$

where z_1 and z_2 are the state variables of the linear system and σ is the new control variable, satisfying,

$$u=\frac{1}{L_gL_f\omega(x)}\left(-L_f^2\omega(x)+\sigma\right) \tag{22}$$

where $L_f^2\omega(x)$ and $L_gL_f\omega(x)$ can be expressed as,

$$L_f^2\omega(x)=\frac{v_{in}^2-x_2v_{in}}{L_2} \tag{23}$$

$$L_gL_f\omega(x)=\frac{v_{in}x_2}{L_2} \tag{24}$$

Since the APF is used to compensate harmonic currents, the current i_{apf}must follow the reference signal i_x fast and precisely. Meanwhile, the voltage v_c should follow the reference value v_{ref}. Similarly, for the system (21), z should follow the reference signal z_{ref} fast and precisely. When the system is stable, according to (20), there is,

$$\begin{cases} \dfrac{1}{2}L_2x_1^2+\dfrac{1}{2}C_2x_2^2=\dfrac{1}{2}L_2i_{ref}^2+\dfrac{1}{2}C_2v_{ref}^2 \\ v_{in}x_1=v_{in}i_{ref} \end{cases} \tag{25}$$

From (25), there is,

$$\begin{cases} x_1=i_{ref} \\ x_2=\pm v_{ref} \end{cases} \tag{26}$$

where x_2 have two solutions, but only one is positive. In the practical system, x_2 is the voltage of C_2 and is positive. So, when z follows z_{ref}, it can guarantee that i_{apf} can follow the reference current i_x, and v_c can follow the reference voltage v_{ref}. Finally, the two control goals (v_{ref} and i_x) can be translated into a control target z_{ref}.

In order to ensure that z follows the reference signal z_{ref}, a state error vector is defined as follows,

$$\begin{cases} e_1=z_1-z_{1ref} \\ e_2=z_2-z_{2ref} \end{cases} \tag{27}$$

where z_{1ref} is the reference signal of z_1, and z_{2ref} is the reference signal of z_2.

According to (21) and (27), there is,

$$\begin{cases} \dot{e}_1=e_2 \\ \dot{e}_2=\sigma-\dot{z}_{2ref} \end{cases} \tag{28}$$

where

$$\dot{z}_{2ref}=v_{in}\left(\frac{v_{in}-v_{ref}}{L_2}+\frac{v_{ref}}{L_2}u\right) \tag{29}$$

Defining the control law,

$$\sigma=\dot{z}_{2ref}-k_1e_1-k_2e_2 \tag{30}$$

According to (28) and (30), there is,

$$\begin{bmatrix}\dot{e}_1\\\dot{e}_2\end{bmatrix}=\begin{bmatrix}0&1\\-k_1&-k_2\end{bmatrix}\begin{bmatrix}e_1\\e_2\end{bmatrix} \tag{31}$$

According to (31), the characteristic equation can be obtained as,

$$A(\lambda)=\begin{bmatrix}-\lambda&1\\-k_1&-k_2-\lambda\end{bmatrix}=\lambda^2+k_2\lambda+k_1=0 \tag{32}$$

where λ is the characteristic root.

When k_1>0 and k_2>0, λ possesses negative real part, the system (31) is stable and the proposed nonlinear unified controller via feedback linearization can follow the target accurately. To analyze the effect of parameters k_1 and k_2 on the controller performance, according to (31), the state variables e_1 and e_2 curves can be obtained as follow,

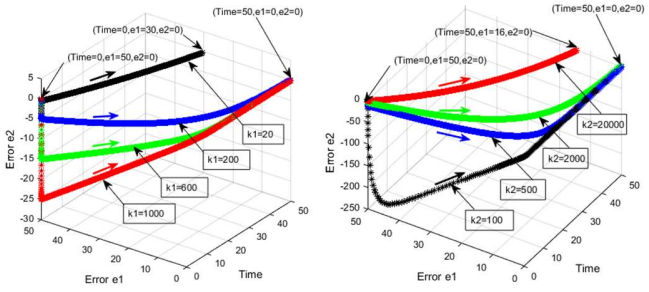

(a) (b)

Fig.10. State variables e_1 and e_2 curves under different parameters k_1 and k_2. (a) k_2 =2000. (b) k_1 =500.

Seen from Fig.10(a), when k_2=2000, with the increase of k_1, the convergence rate of error e_1 gradually increases. The error e_2 first increases then decreases and the fluctuation is bigger when k_1 is bigger. From Fig.10(b), when k_1=500, with the decrease of k_2, the convergence rate of error e_1 gradually increases. The error e_2 first increases then decreases and the fluctuation is bigger when k_2 is smaller. Seen from Fig.10, the error e_1 gradually decreases from 50 to 0 and the error e_2 gradually converges to 0 after an oscillation. As the error e_2 is the derivative of error e_1 and the error e_1=e_2=0 when the system is stable, under the proposed controller, the system can follow the target accurately and the stability is better. When k_1 is smaller and k_2 is bigger, the convergence rate of error e_1 is smaller. In order to improve

This article has been accepted for publication in a future issue of this journal, but has not been fully edited. Content may change prior to final publication. Citation information: DOI 10.1109/TIE.2020.2996147, IEEE Transactions on Industrial Electronics

the tracking speed and accuracy of the target, k_1 should be smaller and k_2 should be larger since e_2 is the derivative of error e_1.

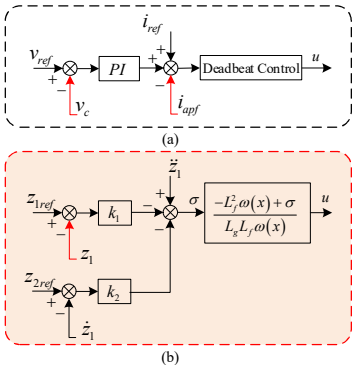

Fig.11. Controller structure of DC-HAPF. (a) The traditional double loop control. (b) The proposed nonlinear unified control.

Based on the analysis above, the traditional double loop control and the proposed nonlinear unified controller via feedback linearization of DC-APF can be shown in Fig.11. Seen from Fig.11(a), for the traditional dual-loop control, the voltage outer loop is generally controlled by PI controller and current inner loop usually adopts the deadbeat control or other control. From Fig.11(b), the proposed nonlinear unified controller is controlled based on the APF's energy, which can realize the unified control of APF's voltage and current. Compared with the traditional double loop control, the proposed nonlinear unified controller is controlled based on the tracking error and the derivative of error simultaneously, and it has better dynamic and steady performance.

Moreover, to analyze the robustness of the proposed controller to the circuit parameters L_2 and C_2, a Lyapunov function is defined as follow,

$$V = \frac{1}{2}\tilde{e}_1^2 + \frac{1}{2k_1}\tilde{e}_2^2 \tag{33}$$

where $\tilde{e}_1$ and $\tilde{e}_2$ are the real state error, expressed as follows,

$$\begin{cases} \tilde{e}_1 = \tilde{z}_1 - z_{1ref} \\ \tilde{e}_2 = \tilde{z}_2 - z_{2ref} \end{cases} \tag{34}$$

where $\tilde{z}_1$ and $\tilde{z}_2$ are the real state variables of z_1 and z_2, respectively. According to (33), due to $k_1>0$, $\tilde{e}_1^2 \geq 0$ and $\tilde{e}_2^2 \geq 0$, there is $V \geqslant 0$.

Differentiating (33), there is,

$$\dot{V} = \tilde{e}_1\dot{\tilde{e}}_1 + \frac{1}{k_1}\tilde{e}_2\dot{\tilde{e}}_2 \tag{35}$$

According to (28), (30) and (34), there is,

$$\begin{cases} \dot{\tilde{e}}_1 = \tilde{e}_2 \\ \dot{\tilde{e}}_2 = -k_1\tilde{e}_1 - k_2\tilde{e}_2 \end{cases} \tag{36}$$

Substituting (36) into (35), there is,

$$\begin{aligned} \dot{V} &= \tilde{e}_1\tilde{e}_2 + \frac{1}{k_1}\tilde{e}_2\left(-k_1\tilde{e}_1 - k_2\tilde{e}_2\right) \\ &= \frac{-k_2}{k_1}\tilde{e}_2^2 \leq 0 \end{aligned} \tag{37}$$

See from (37), only when the $\tilde{e}_2 = 0$, there is $\dot{V}$=0. Therefore, according to the Lyapunov theory, the system is stable. When the system is stable, there is,

$$\begin{cases} \tilde{e}_1 = \dfrac{1}{2}\left[\left(L_2+\Delta L_2\right)i_{apf}^2 + \left(C_2+\Delta C_2\right)v_c^2 - L_2 i_{ref}^2 - C_2 v_{ref}^2\right] = 0 \\ \tilde{e}_2 = v_{in}i_{apf} - v_{in}i_{ref} = 0 \end{cases} \tag{38}$$

where ΔL_2 and ΔC_2 are the parameter errors of L_2 and C_2, respectively.

From (38), when $\tilde{e}_2$=0, there is i_{apf}= i_{ref}; when $\tilde{e}_1$=0, there will be a fixed error for the dc voltage v_c. Moreover, when the real circuit parameter L_2 or C_2 is bigger, the dc voltage v_c will be slightly smaller than v_{cref}; when the real parameter is smaller, the dc voltage v_c will be slightly bigger than v_{cref}. Based on the analysis above, the circuit parameter error only affects the control of the dc voltage v_c and it does not affect the harmonic suppression effect of the DC-HAPF. Therefore, the proposed controller can suppress the harmonic current effectively, and has a strong robustness to circuit parameters L_2 and C_2.

IV. EXPERIMENTS

To validate the feasibility of the proposed DC-HAPF and nonlinear unified controller via feedback linearization, a prototype for single-stage single-phase inverter with DC-HAPF is built in lab for verification, and the proposed control strategy is implemented in TMS320F28335. Fig.12 gives the schematic diagram of this single-stage single-phase inverter with DC-HAPF. The parameters of circuit are shown in Table I and the parameters of controllers are shown in Table II. The experimental results are shown as follows.

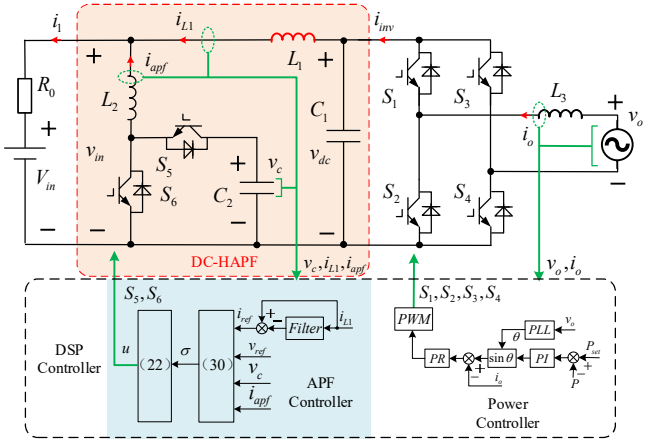

Fig.12. Schematic diagram of the prototype.

Firstly, the harmonic suppression performances of four different kinds of filters are compared and shown in Fig.13. Compared with Fig.13(a) with filter C, the current i_1 in Fig.13(b) with filter CL mainly has the SHC and less high-frequency harmonic currents. So, the switching harmonic currents can be effectively suppressed by CL filter. Seen from Fig.13(c) with filter C+APF, the SHC is suppressed. As the active power filter is difficult to suppress the high-frequency harmonics, the current i_1 still has lots of high frequency harmonic components. From Fig.13(d) with filter CL+APF, the SHC and switching harmonics in the current i_1 are greatly suppressed and the current i_1 are much better than that of Fig.13 (b) and (c). So, the proposed DC-HAPF can effectively suppress the harmonic currents at the dc-side of single-phase inverter. Note that the current THD with C+APF is lower than that with filter C and higher than that with

This article has been accepted for publication in a future issue of this journal, but has not been fully edited. Content may change prior to final publication. Citation information: DOI 10.1109/TIE.2020.2996147, IEEE Transactions on Industrial Electronics

filter CL since there are lots of high frequency switching harmonics. However, with the work of filter CL+APF, the THD of dc current i_1 is less than 5% and is the lowest. From Fig.13, the passive filter CL can effectively suppress the high-frequency harmonics, and it is helpful for the active power filter to compensate the low frequency harmonic currents. Therefore, the DC-HAPF can effectively suppress the lower- and high-frequency harmonic currents at the dc-side of single-phase inverter, which integrates the merits of active power filter and passive power filter.

TABLE I
PARAMETERS OF CIRCUIT

Parameter	Value
Voltage of DC voltage source V_{in} /V	48
Internal resistance of DC power R_0/Ω	0.01
Capacitance of CL filter C_1 /mF	1.5
Inductance of CL filter L_1 /mH	0.1
Capacitance of active power filter C_2/mF	2
Inductance of active power filter L_2/mH	1.5
AC voltage v_{ac}/V	50
Inductance L_3 /mH	2

TABLE II
PARAMETERS OF CONTROLLERS

Parameter	Value
Rated active power P_{set} /W	500
Rated reactive power Q_{set} /W	0
PI controller parameter K_P	0.001
PI controller parameter K_I	1
PR controller parameter K_{PP}	0.5
PR controller parameter K_{PR}	500
Capacitance voltage v_{ref}/V	65
PWM switching frequency f_{pwm}/kHz	10
Sampling frequency f_s/kHz	10
Controller parameter k_1	1
Controller parameter k_2	20000

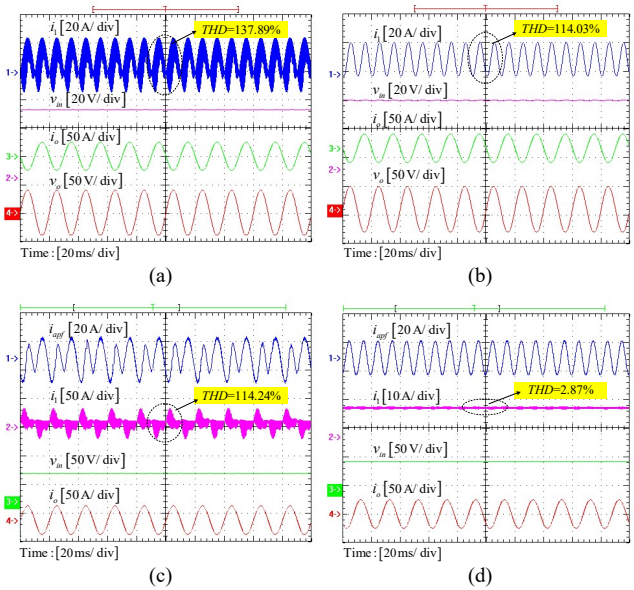

Fig.13. Experimental waveforms with different filters. (a)With filter C. (b) With filter CL. (c) With filter C+APF. (d) With filter CL+APF.

Fig.14 shows the experimental waveforms when the DC-HAPF is controlled by different control methods. Seen from Fig.14(a), adopting the traditional deadbeat control, the current i_1 has two oscillation processes when the power changes suddenly. When the power doubles suddenly, there will be a big input error and a longer response time since the voltage outer loop is controlled by PI controller. Fig.14(b) shows the experimental waveforms under the sliding mode control, where the current inner loop is controlled by sliding mode controller and the voltage outer loop is controlled by PI controller. As seen from Fig14(b), although the sliding mode control has good dynamic performance, the current i_1 also has an oscillation process because of the current reference is affected by the voltage PI controller. From Fig14(c), adopting the nonlinear unified controller, since the voltage and current dual-loop control is converted to a single-loop control of energy, the current i_1 basically has no oscillation process when the power changes suddenly. In addition, as the proposed controller is designed based on the tracking error and the derivative of error, the DC-HAPF can attenuate the tracking error fast, and the THD of dc current i_1 is 2.87% and the lowest. Based on the analysis above, the steady and dynamic performances of the proposed nonlinear unified control are better than the ones of traditional deadbeat control and sliding mode control.

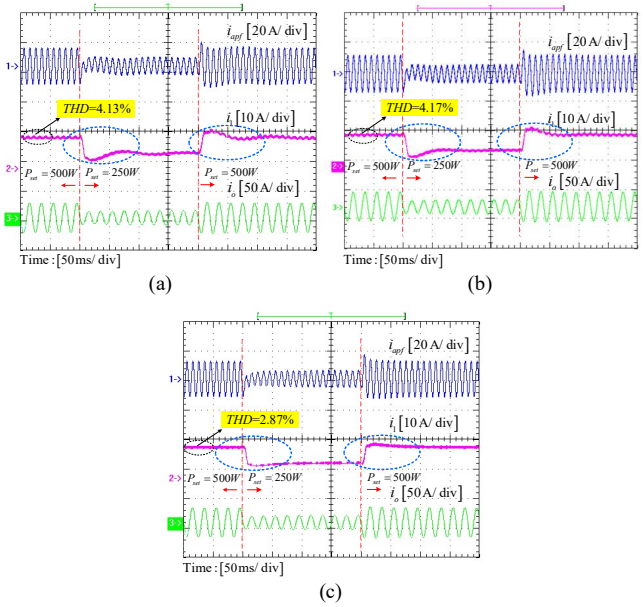

Fig.14. Experimental waveforms under different control methods. (a) Deadbeat control. (b) Sliding mode control. (c) Proposed nonlinear unified control.

Fig.15(a) shows the experimental waveforms under the different parameter k_1. When k_1 increases from 1 to 20000 suddenly, the THD of waveform of dc current i_1 decreases from 4.92% to 3.49%. Fig.15(b) shows the experimental waveforms under the different parameter k_2. When k_2 increases from 2000 to 20000 suddenly, the THD of waveform of dc current i_1 decreases from 4.94% to 2.87% and the waveform is smoother. No matter increase k_1 or k_2, the THD of dc current i_1 will decreases. Since the parameter k_2 is the coefficient of e_2 in the controller and e_2 is the derivative of e_1, the target tracking error e_1 reduces faster and the steady state error is smaller when k_2 is bigger. Therefore, the THD of dc current i_1 is smaller when k_1=1 and k_2=20000. In addition, to analyze the influence of the parameter D_k on filtering performance, as the duty ratio of converter is directly proportional to v_{ref}, here it will change v_{ref} to show the influence on the operation performance of DC-HAPF. Seen from Fig.15(c), when v_{ref} is decreased from 100V to 60V, the high-frequency harmonic current in i_{apf} decreases gradually

This article has been accepted for publication in a future issue of this journal, but has not been fully edited. Content may change prior to final publication. Citation information: DOI 10.1109/TIE.2020.2996147, IEEE Transactions on Industrial Electronics

and the waveform of dc current i_1 becomes better gradually. When the system is stable, the capacitor voltage v_c will be equal to v_{ref}. With the decrease of voltage v_c, the change value of current i_{apf} will decrease in the same switching cycle, and then the distortion of current i_{apf} will be narrow. Therefore, the waveform of dc current i_1 is better when v_{ref}=60V.

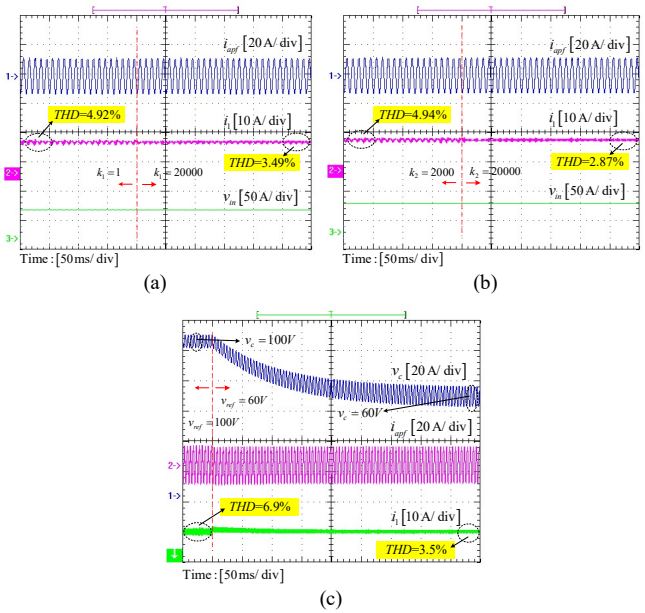

Fig.15. Experimental waveforms under different control parameters. (a) Under different $k_1$when k_2=2000. (b) Under different k_2 when k_1=1. (b) Under different v_{ref}.

In DC-HAPF, the inductance L_1 is very important for the high frequency harmonic current suppression. The experimental waveforms with different L_1 can be obtained, as shown in Fig.16.

As seen from Fig.16(a), when the value of L_1 is changed from 0.1mH to 1mH, the waveforms of i_{apf} and i_1 both occur oscillation. According to Fig16(b), when the value of L_1 is changed from 0.1mH to 0.01mH, the current i_1 also becomes worse and it has large amount of high frequency harmonic current. When the value of L_1 is bigger, L_1 will hinder the transmission of electrical energy. When the value of L_1 is smaller, L_1 cannot effectively filter out the high frequency harmonic current. So, no matter the value of inductance L_1 is too big or too small, the quality of current i_1 will be deteriorated. When the value of L_1 changes, the current i_{L1} changes and it will affect the harmonic control effect of active filters. To better suppress harmonics, an appropriate inductance L_1 is important.

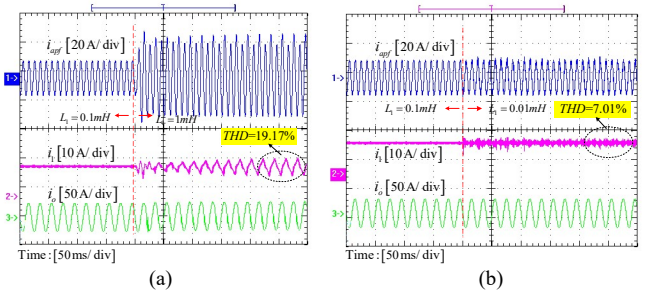

Fig.16. Experimental waveforms under different L_1. (a)Increase L_1 from 0.1mH to 1mH. (b)Decrease L_1 from 0.1mH to 0.01mH.

Fig.17 shows the experimental waveforms under the disturbance of parameter L_2 or C_2. Seen form Fig.17(a), when L_2 is increased by 20% suddenly, the changed value of current i_{apf} will decrease at the same switching cycle, and then the output harmonic current will slightly decrease. Therefore, the harmonic suppression effect of DC-HAFP becomes better and the THD of dc current i_1 becomes lower. Seen form Fig.17(b), when L_2 is decreased suddenly, the changed value of current i_{apf} will increase at the same switching cycle, and then the output harmonic current will slightly rise. Therefore, the harmonic suppression effect of DC-HAFP becomes worse and the THD of dc current i_1 becomes higher. From Fig.17(a) and Fig.17(b), no matter parameter L_2 is bigger or smaller than normal value, the harmonic currents can be effectively suppressed by DC-HAPF and the system is stable. As seen from Fig.17(c), when C_2 is increased by 20%, the fluctuations of dc voltage v_c will decrease, and then the harmonic suppression effect of DC-HAPF will be slightly better. Meanwhile, the dc voltage v_c becomes slightly smaller, which is consistent with the robustness analysis in Section III. Seen from Fig.17(d), when C_2 is decreased by 20%, the fluctuations of dc voltage v_c will increase, and then the harmonic suppression effect of DC-HAPF will be slightly worse. Meanwhile, the dc voltage v_c slightly becomes bigger, which is also consistent with the robustness analysis in Section III. From Fig.17(c) and Fig.17(d), no matter parameter C_2 is bigger or smaller than normal value, the harmonic currents can be effectively suppressed by DC-HAPF. Compared with the parameter C_2, the parameter L_2 has a greater impact on the performance of the controller. Therefore, the DC-HAPF with nonlinear unified controller via feedback linearization has a strong robustness since the proposed controller is regulated based on the tracking error and the derivative of error.

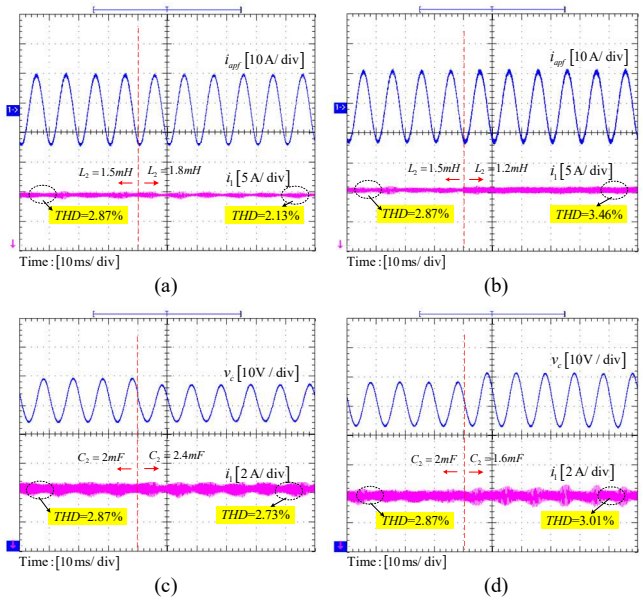

Fig.17. Experimental waveforms under different L_2 or C_2. (a) +20% change of L_2. (b) -20% change of L_2. (c) +20% change of C_2. (d) -20% change of C_2.

V. Conclusion

In order to solve the dc side harmonic problem and distinguish traditional ac hybrid active filter, this paper proposed the concept of DC-HAPF. For suppressing the harmonic current at

the dc side of the single-stage single-phase inverter, a dc hybrid active power filter structure is presented, which integrates the merits of active power filter and passive power filter. Moreover, a nonlinear unified controller is proposed by applying feedback linearization theory, where the voltage and current dual-loop control is converted to a single-loop control of energy. Since the proposed controller is controlled based on the tracking error and the derivative of error, the DC-HAPF can attenuate the tracking error fast, and the robustness of the proposed controller is good. The proposed energy-based controller also has potential application value in other scenarios, which can improve the controller's performance by converting the typical voltage and current dual-loop control into a single-loop control of energy.

REFERENCE

[1] M. Vitorino, L. Alves, R. Wang, and M. Correa, "Low-frequency power decoupling in single-phase applications: A comprehensive overview," *IEEE Trans. Power Electron.*, vol. 32, no. 4, pp. 2892-2912, Apr. 2017.

[2] H. Hu, S. Harb, N. Kutkut, I Batarseh, and Z. Shen, "A review of power decoupling techniques for microinverters with three different decoupling capacitor locations in PV systems," *IEEE Trans. Power Electron.*, vol. 28, no. 6, pp. 2711-2726, Jun. 2013.

[3] W. Wang, X. Ruan, "A Modified Reference of an Intermediate Bus Capacitor Voltage-Based Second-Harmonic Current Reduction Method for a Standalone Photovoltaic Power System," *IEEE Trans. Power Electron.*, vol. 31, no. 8, pp. 5562-5573, Aug. 2016.

[4] L. Zhang, X. Ruan, X. Ren, "Second Harmonic Current Reduction for Two-Stage Inverter With Boost-Derived Front-End Converter: Control Schemes and Design Considerations," *IEEE Trans. Power Electron.*, vol. 33, no. 7, pp. 5562-5573, Jul. 2018.

[5] Z. Wei, X. Deng, C. Gong, J. Chen, and F. Zhang, "A novel technique of low frequency input current ripple reduction in two-stage dc-ac inverter," in *Proc. IEEE Ind. Electron. Conf.*, 2012, pp. 139–143.

[6] A. Ahmad, A. Abrishamifar, and S. Samadi, "Low-frequency current ripple reduction in front-end boost converter with single-phase inverter load," *IET Power Electron.*, vol. 5, no. 9, pp. 1676–1683, May 2012.

[7] Y. Shi, B. Liu, and S. Duan, "Low-frequency input current ripple reduction based on load current feedforward in a two-stage single-phase inverter," *IEEE Trans. Power Electron.*, vol. 31, no. 11, pp. 7972–7985, Nov. 2016.

[8] W. Wang and X. Ruan, "A modified reference of an intermediate bus capacitor voltage-based second-harmonic current reduction method for a standalone photovoltaic power system," *IEEE Trans. Power Electron.*, vol. 31, no. 8, pp. 5562–5573, Aug. 2016.

[9] L. Zhang, X. Ren, and X. Ruan, "A band-pass filter incorporated into the inductor current feedback path for improving dynamic performance of the front-end dc-dc converter in two-stage inverter," *IEEE Trans. Ind. Electron.*, vol. 61, no. 5, pp. 2316–2325, May 2014.

[10] G. Zhu, X. Ruan, L. Zhang, and X. Wang, "On the reduction of second harmonic current and improvement of dynamic response for two-stage single-phase inverter," *IEEE Trans. Power Electron.*, vol. 30, no. 2, pp. 1028–1041, Feb. 2015.

[11] G.-R. Zhu, S.-C. Tan, Y. Chen, and C. Tse, "Mitigation of low-frequency current ripple in fuel-cell inverter systems through waveform control," *IEEE Trans. Power Electron.*, vol. 28, no. 2, pp. 779–792, Feb. 2013.

[12] D. B. W. Abeywardana, B. Hredzak, and V. G. Agelidis, "An input current feedback method to mitigate the dc-side low-frequency ripple current in a single-phase boost inverter," *IEEE Trans. Power Electron.*, vol. 31, no. 6, pp. 4594–4603, Jun. 2016.

[13] S. Li, G.-R. Zhu, S.-C. Tan, and S. Hui, "Direct ac/dc rectifier with mitigated low-frequency ripple through inductor-current waveform control," *IEEE Trans. Power Electron.*, vol. 30, no. 8, pp. 4336–4348, Aug. 2015.

[14] W. Yao, X. Zhang, X. Wang, Y. Tang, P. C. Loh, and F. Blaabjerg, "Power decoupling with autonomous reference generation for single-phase differential inverters," in *Proc. 17th Eur. Conf. Power Electron.* Appl., 2015, pp. 1–10.

[15] PT. Krein, RS. Balog, M. Mirjafari, "Minimum Energy and Capacitance Requirements for Single-Phase Inverters and Rectifiers Using a Ripple Port," *IEEE Trans. Power Electron.*, vol. 27, no. 11, pp. 4690–4698, Nov. 2012.

[16] R. Wang, F. Wang, D. Boroyevich, R. Burgos, R. Lai, P. Ning, K. Rajashekara, "A High Power Density Single-Phase PWM Rectifier With Active Ripple Energy Storage," *IEEE Trans. Power Electron.*, vol. 26, no. 5, pp. 1430–1443, May. 2011.

[17] I. Serban and C. Marinescu, "Active power decoupling circuit for a single-phase battery energy storage system dedicated to autonomous microgrids," in *Proc. IEEE Int. Symp. Ind. Electron.*, 2010, pp. 2717–2722.

[18] W. Cai, B. Liu, S. Duan, and L. Jiang, "An active low-frequency ripple control method based on the virtual capacitor concept for BIPV systems," *IEEE Trans. Power Electron.*, vol. 29, no. 4, pp. 1733–1745, Apr. 2014.

[19] M. Vitorino, M. Correa, and C. Jacobina, "Single-phase power compensation in a current source converter," in *Proc. IEEE Energy Convers. Congr. Expo.*, 2013, pp. 5288–5293.

[20] H. Han, Y. Liu, Y. Sun, M. Su, and W. Xiong, "Single-phase current source converter with power decoupling capability using a series connected active buffer," *IET Power Electron.*, vol. 8, no. 5, pp. 700–707, May, 2015.

[21] Y. Ohnuma and J.-I. Itoh, "Comparison of boost chopper and active buffer as single to three phase converter," in *Proc. IEEE Energy Convers. Congr. Expo.*, 2011, pp. 515–521.

[22] H. A. Zarchi, J. Soltani, and G. A. Markadeh, "Adaptive input–output feedback-linearization-based torque control of synchronous reluctance motor without mechanical sensor," *IEEE Trans. Ind. Electron.*, vol. 57, no. 1, pp. 375–384, Jan. 2010.

[23] P. Liutanakul, S. Pierfederici, and F. M. Tabar, "Application of SMC with I/O feedback linearization to the control of the cascade controlled rectifier/inverter-motor drive system with small dc-link capacitor," *IEEE Trans. Power Electron.*, vol. 23, no. 5, pp. 2489–2499, Sep. 2008.

[24] C. Lascu, I. Boldea, and F. Blaabjerg, "Direct torque control via feedback linearization for permanent magnet synchronous motor drives," in *Proc.Int. Conf. Optim. Electr. Electron. Equipment*, 2012, pp. 338–343.

[25] F. Chen, Z. Chen, H. Wang, J. Le, "Research of State Exact Feedback Linearization Control of Shunt Single-Phase Active Power Filter," in *Proic, APPEEC.*, Mar, 2010, pp.1-4.

[26] C. Lascu, S. Jafarzadeh, MS. Fadali, F. Blaabjerg, "Direct Torque Control With Feedback Linearization for Induction Motor Drives," *IEEE Trans. Power Electron.*, vol. 32, no.3, pp. 2072–2080, Mar. 2017.

[27] J. Miret, LGD. Vicuna, J. Matas, JM. Guerrero, J. Cruz, "Simplified feedback linearization of a single-phase active power filter using sliding mode control," in *Proic, IEEE ISIE*, 2004, pp.869-873.

[28] X. Bao, F. Zhuo, Y. Tian, P. Tan, "Simplified Feedback Linearization Control of Three-Phase Photovoltaic Inverter With an LCL Filter," *IEEE Trans. Power Electron.*, vol. 28, no.6, pp. 2739–2752, Jun. 2013.

[29] M. A. Mahmud, M. J. Hossain, H. R. Pota, and N. K. Roy, "Robust Nonlinear Controller Design for Three-Phase Grid-Connected Photovoltaic Systems Under Structured Uncertainties," *IEEE Trans. Power Del.*, vol. 29, no.3, pp. 1221–1230, Jun. 2014.

[30] M. A. Mahmud, H. R. Pota, and M. J. Hossain, "Nonlinear DSTATCOM controller design for distribution network with distributed generation to enhance voltage stability," *Int. J. Elect. Power Energy Syst.*, vol. 53, pp. 974–979, Dec. 2013.

[31] M. A. Chowdhury, and G. M, "Shafiullah. SSR Mitigation of Series-Compensated DFIG Wind Farms by a Nonlinear Damping Controller Using Partial Feedback Linearization," *IEEE Trans. Power Syst.*, vol. 33, no.3, pp. 2528–2538, May. 2018.

Gaoxiang Li was born in Henan, China, 1990. He received the B.S. degree in electrical engineering and automation from the School of Electrical Engineering and Automation, Henan Polytechnic University, Jiaozuo, China, in 2014. He received the M.S. degree in electrical engineering from the College of Information science and Engineering, Central South University, Changsha, China, in 2017. Currently, he has been working toward the Ph.D. degree in electrical engineering from the College of Electrical and Information Engineering, Hunan University, Changsha, China.

His research interests include power quality control, new energy generation, sub-synchronous oscillation suppression.

An Luo (SM'09) was born in Changsha, China, in 1957. He received the B.S. and M.S. degrees in industrial automation from Hunan University, Changsha, in 1982 and 1986, respectively, and the Ph.D. degree in fluid power transmission and control from Zhejiang University, Hangzhou, China, in 1993. Between 1996 and 2002, he was a Professor with Central South University. Since 2003, he has been a Professor in the College of Electrical and Information Engineering, Hunan University, where he also serves as the Chief of National Electric Power Conversion and Control Engineering Technology Research Center.

His research interests mainly include distributed generation, microgrid, and power quality. He was elected to the Chinese National Academy of Engineering (CNAE) in 2015, the highest honor for scientists and engineers and scientists in China. He has won the highly prestigious China National Science and Technology Awards three times (2014, 2010 and 2006).

Zhixing He (S'15- M'17) was born in Hunan, China, 1989. He received the B.S. degree in information science and Engineering from Central South University, Changsha, China, in 2011, and the Ph.D. degree in electrical engineering from Hunan University, Changsha, China, in 2017. Currently, he has been working an Associate Professor in electrical engineering from Hunan University, Changsha, China.

His research interests include power electronics, and modular multilevel converter.

Fujun Ma (M'15) was born in Hunan, China, 1985. He received the B.S. degree in Automation and Ph.D. degree in Electrical Engineering from Hunan University, Changsha, in 2008 and 2015, respectively. Since 2016, he has been an Associate Professor with the College of Electrical and Information Engineering, Hunan University. His research interests include power quality managing technique of electrified railway, electric power saving, reactive power compensation, and active power filters.

Yandong Chen (M'14-SM'18) was born in Hunan, China, in 1979. He received the B.S. and M.S. degree in instrument science and technology from Hunan University, Changsha, China, in 2003 and 2006, respectively, and the Ph.D. degree in electrical engineering from Hunan University, Changsha, China, in 2014. He has been a Professor in the College of Electrical and Information Engineering, Hunan University, Changsha.

His research interests include power electronics for microgrid, distributed generation, power quality, and energy storage. Dr. Chen is a recipient of the 2014 National Technological Invention Awards of China, and the 2014 WIPO-SIPO Award for Chinese Outstanding Patented Invention. He is a member of IEEE Power Electronics Society.

Wenhua Wu (S'16) was born in Hunan, China, 1991. He received the B.S. and Ph.D. degree from the College of Electrical and Information Engineering, Hunan University, Changsha, China, in 2014 and 2019, respectively. Currently, he has been working postdoctoral research in electrical engineering from Hunan University, Changsha, China.

His research interests include renewable energy generation systems, microgrid, power quality, and VSC-HVDC systems.

Zhen Zhu was born in Hunan, China, 1988. He received the B.S. degree and the M.S. degree in Automation from College of Geophysics and Information Engineering, China University of Petroleum, Beijing, China, in 2013 and 2017, respectively. He has been working toward the Ph.D. degree in Electrical Engineering in the College of Electrical and Information Engineering, Hunan University, Changsha since 2017.

His research interests include hybrid compensation of traction system and energy management of energy router.

Josep M. Guerrero (S'01-M'04-SM'08-FM'15) received the B.S. degree in telecommunications engineering, the M.S. degree in electronics engineering, and the Ph.D. degree in power electronics from the Technical University of Catalonia, Barcelona, in 1997, 2000 and 2003, respectively. Since 2011, he has been a Full Professor with the Department of Energy Technology, Aalborg University, Denmark. From 2015 he is a distinguished guest Professor in Hunan University. His research interests mainly include power electronics, distributed energy-storage, and microgrids. Prof. Guerrero is an Associate Editor for the IEEE TRANSACTIONS ON POWER ELECTRONICS, the IEEE TRANSACTIONS ON INDUSTRIAL ELECTRONICS, and the IEEE Industrial Electronics Magazine, and an Editor for the IEEE TRANSACTIONS on SMART GRID and IEEE TRANSACTIONS on ENERGY CONVERSION. In 2014, 2015, and 2016 he was awarded by Thomson Reuters as Highly Cited Researcher, and in 2015 he was elevated as IEEE Fellow for his contributions on distributed power systems and microgrids.